Korean Chem. Eng. Res., 54(6), 734-745 (2016)
http://dx.doi.org/10.9713/kcer.2016.54.6.734
PISSN 0304-128X, EISSN 2233-9558

총 설

Review on the Determination of Frumkin, Langmuir, and Temkin Adsorption Isotherms at Electrode/Solution Interfaces Using the Phase-Shift Method and Correlation Constants

Jinyoung Chun and Jang H. Chun*,†

Department of Chemical Engineering, Pohang University of Science and Technology, 77, Cheongam-ro, Nam-gu, Pohang, Gyeongbuk, 37673, Korea
**President, Kwangwoon University, 20, Gwangun-ro, Nowon-gu, Seoul, 01897, Korea*
(Received 1 September 2016; accepted 27 September 2016)

Abstract – This review article described the electrochemical Frumkin, Langmuir, and Temkin adsorption isotherms of over-potentially deposited hydrogen (OPD H) and deuterium (OPD D) for the cathodic H_2 and D_2 evolution reactions (HER, DER) at Pt, Ir, Pt-Ir alloy, Pd, Au, and Re/normal (H_2O) and heavy water (D_2O) solution interfaces. The Frumkin, Langmuir, and Temkin adsorption isotherms of intermediates (OPD H, OPD D, etc.) for sequential reactions (HER, DER, etc.) at electrode/solution interfaces are determined using the phase-shift method and correlation constants, which have been suggested and developed by Chun et al. The basic procedure of the phase-shift method, the Frumkin, Langmuir, and Temkin adsorption isotherms of OPD H and OPD D and related electrode kinetic and thermodynamic parameters, i.e., the fractional surface coverage ($0 \le \theta \le 1$) vs. potential (E) behavior (θ vs. E), equilibrium constant (K), interaction parameter (g), standard Gibbs energy (ΔG_θ°) of adsorption, and rate (r) of change of ΔG_θ° with θ ($0 \le \theta \le 1$), at the interfaces are briefly interpreted and summarized. The phase-shift method and correlation constants are useful and effective techniques to determine the Frumkin, Langmuir, and Temkin adsorption isotherms and related electrode kinetic and thermodynamic parameters (θ vs. E, K, g, ΔG_θ°, r) at electrode/solution interfaces.

Key words: Phase-shift method and correlation constants, Frumkin, Langmuir, Temkin adsorption isotherms, Over-Potentially deposited hydrogen and deuterium, Noble metal alloy electrodes

1. Introduction

Many experimental methods have been developed and used to study the adsorption of hydrogen for the cathodic H_2 evolution reaction (HER) at noble metal and alloy/aqueous solution interfaces [1-7]. The cathodic HER is one of the most extensively studied topics in electrochemistry, electrocatalysis, hydrogen technologies, and fuel cells, etc. It is well known that under-potentially deposited hydrogen (UPD H) and over-potentially deposited hydrogen (OPD H) occupy different surface adsorption sites and act as two distinguishable electroadsorbed H species, and that only OPD H can contribute to the cathodic HER [2-7]. However, there is not much reliable data on the Frumkin, Langmuir, and Temkin adsorption isotherms of OPD H for the cathodic HER and related electrode kinetic and thermodynamic parameters, i.e., the fractional surface coverage ($0 \le \theta \le 1$) vs. potential (E) behavior (θ vs. E), equilibrium constant (K), interaction parameter (g), standard Gibbs energy (ΔG_θ°) of adsorption, and rate (r) of change of ΔG_θ° with θ ($0 \le \theta \le 1$). Furthermore, there is not much reliable data on the Frumkin, Langmuir, and Temkin adsorption isotherms of over-potentially deposited deuterium (OPD D) for the cathodic D_2 evolution reaction (DER) and related electrode kinetic and thermodynamic parameters. Similarly, there is not much reliable data on the Frumkin, Langmuir, and Temkin adsorption isotherms of hydroxide (OH) and deuteroxide (OD) for the anodic O_2 evolution reaction (OER) and related electrode kinetic and thermodynamic parameters. Because, to the authors' knowledge, K and g for the Frumkin adsorption isotherms of intermediates cannot be experimentally and readily determined using conventional methods [1-7]. Also, a quantitative relationship between the Temkin and Frumkin or Langmuir adsorption isotherms of intermediates has not been developed or reported to study the cathodic HER and DER or the anodic OER. Thus, there is a technological need for a useful, effective, and reliable method to determine the Frumkin, Langmuir, and Temkin adsorption isotherms of intermediates (OPD H, OPD D, OH, OD, etc.) for the sequential reactions (HER, DER, OER, etc.) and related electrode kinetic and thermodynamic parameters at the interfaces.

Although the Frumkin and Langmuir adsorption isotherms may be regarded as classical models and theories, it is preferable to consider the Frumkin and Langmuir adsorption isotherms for OPD H and OPD D rather than electrode kinetics and thermodynamics equations for OPD H and OPD D because these adsorption isotherms are associated more directly with the atomic mechanism of OPD H and OPD D. To determine the Frumkin, Langmuir, and Temkin adsorption isotherms, the phase-shift method and correlation constants have been originally suggested and developed on the basis of relevant experimental results and physical phenomena rather than mathematical

† To whom correspondence should be addressed.
E-mail: jhchun@kw.ac.kr
‡ This article is dedicated to Prof. Choon Han on the occasion of his retirement from Kwangwoon University.

formalisms of electrochemistry and electrochemical impedance spectroscopy (EIS) [8]. The phase-shift method is a unique EIS technique for studying the linear relationship between the phase shift ($90° \geq -\varphi \geq 0°$) vs. potential ($E$) behavior for the optimum intermediate frequency (f_o) and the fractional surface coverage ($0 \leq \theta \leq 1$) vs. potential (E) behavior of intermediates (UPD H, OPD H, OPD D, OH, OD, etc.) for sequential reactions (HER, DER, OER, etc.) at noble and highly corrosion-resistant metal and alloy/solution interfaces [9-21]. The (θ vs. E) behavior is well known as the Frumkin or Langmuir adsorption isotherm.

Many scientific phenomena have been interpreted by their behavior rather than by their nature. For example, the wave-particle duality of light and electrons, i.e., their wave and particle behaviors, is well known in science and has been applied in engineering. At first glance, it seems that there is no linear relationship between the ($-\varphi$ vs. E) behavior for f_o and the (θ vs. E) behavior at the interfaces. Thus, tedious experimental techniques and procedures [9-13] have been used to verify the validity and correctness of the phase-shift method. A new method must be rigorously tested, especially when it is unique, but only with pure logic and objectivity and through scientific procedures. However, the objections to the phase-shift method do not fulfill these criteria (see Text and Supporting Information in Ref. 18). The comments and replies on the phase-shift method are briefly summarized elsewhere [18-20]. In recent, the validity of the phase-shift method has been qualitatively analyzed and verified by Garcia et al. [22].

In this review article, we supplement and summarize the Frumkin, Langmuir, and Temkin adsorption isotherms of OPD H and OPD D and related electrode kinetic and thermodynamic parameters (θ vs. E, K, g, ΔG_θ°, r) at noble metal (Pt, Ir, Pd, Au, Re) and alloy (Pt-Ir)/normal (H_2O) and heavy water (D_2O) solution interfaces [9-21].

2. Theoretical and Experimental Backgrounds of the Phase-Shift Method

2-1. The equivalent circuit for the adsorption and sequential reactions

The equivalent circuit for the adsorption of OPD H and OPD D for the cathodic HER and DER at the Pt, Ir, Pt-Ir alloy, Pd, Au, and Re/H_2O and D_2O solution interfaces can be expressed as shown in Fig. 1a [18-20,23-25]. In Fig. 1a, R_S is the real solution resistance; R_F is the real resistance due to the faradaic resistance (R_ϕ) for the discharge step and superposition of various effects; R_P is the real resistance due to the faradaic resistance (R_R) for the recombination step and superposition of various effects; C_P is the real capacitance due to the adsorption pseudocapacitance (C_ϕ) for the discharge step and superposition of various effects; and C_D is the real double-layer capacitance. Correspondingly, neither R_F nor C_P is constant; both R_F and C_P depend on E and θ and can be measured. Note that both R_ϕ and C_ϕ also depend on E and θ but cannot be measured.

The numerical derivation of C_ϕ from the Frumkin and Langmuir adsorption isotherms is described elsewhere, and R_ϕ depends on C_ϕ [23-25]. They attain maximum values at $\theta \approx 0.5$ and intermediate E, decrease symmetrically with E at other values of θ, and approach minimum values or 0 at $\theta \approx 0$ and low E and $\theta \approx 1$ and high E. This behavior is well known in interfacial electrochemistry, electrode kinetics, and EIS. The unique feature and combination of R_ϕ and C_ϕ vs. E, i.e., $-\varphi$ and θ vs. E, imply that the normalized rate of change of $-\varphi$ with respect to E, i.e., $\Delta(-\varphi)/\Delta E$, corresponds to that of θ with respect to E, i.e., $\Delta\theta/\Delta E$, and vice versa (see Footnotes *c* and *d* in Table 1). This is a typical characteristic of the Gaussian profiles of $\Delta(-\varphi)/\Delta E$ and $\Delta\theta/\Delta E$, i.e., the Frumkin and Langmuir adsorption isotherms. Note that φ depends on both E and frequency (f) but θ depends on only E [25]. The linear relationship between the Gaussian profiles of $\Delta(-\varphi)/\Delta E$ and $\Delta\theta/\Delta E$ most clearly appears at the specified intermediate frequency. We refer to it as the optimum intermediate frequency (f_o). The value of f_o is experimentally and graphically evaluated on the basis of $\Delta(-\varphi)/\Delta E$ and $\Delta\theta/\Delta E$ for intermediate and other frequencies (see Fig. 9).

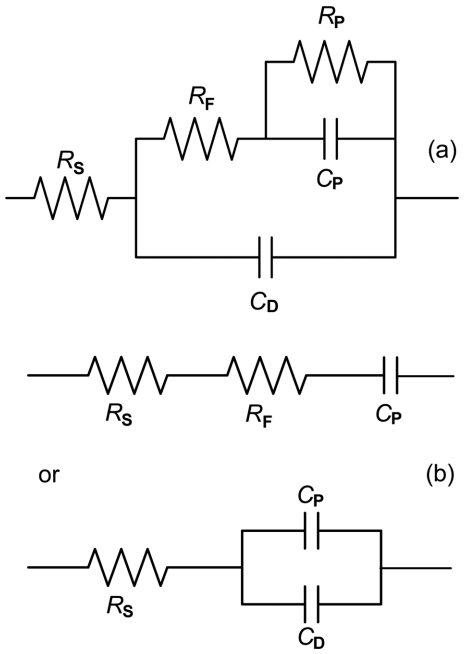

Fig. 1. (a) Experimentally proposed equivalent circuit for the phase-shift method. (b) Simplified equivalent circuits for intermediate frequency responses.

2-2. The frequency response of the equivalent circuit for the adsorption

The frequency responses of the equivalent circuit for all f that is shown in Fig. 1a are essential for understanding the unique feature and combination of (R_S, R_F) and (C_P, C_D) vs. E for f_o, i.e., the linear relationship between the ($-\varphi$ vs. E) behavior for f_o and the (θ vs. E) behavior. At low frequencies, the equivalent circuit for all f can be expressed as a series circuit of R_S, R_F, and R_P. At high frequencies, the equivalent circuit for all f can be expressed as a series circuit of R_S and C_D. Both the low and high frequency responses are meaning-

less for studying the adsorption of OPD H and OPD D. Note that R_F and C_P include R_ϕ and C_ϕ, i.e., the adsorption of OPD H and OPD D, respectively. At intermediate frequencies, one finds regions in which the equivalent circuit for all f behaves as a series circuit of R_S, R_F, and C_P or a series and parallel circuit of R_S, C_P, and C_D, as shown in Fig. 1b. However, the simplified equivalent circuit shown in Fig. 1b does not represent the change of the cathodic HER and DER themselves but only the intermediate-frequency response.

At intermediate frequencies, the impedance (Z) and lagged phase-shift ($-\varphi$) are given by [16-20,23,25]

$$Z = R_S + R_F - \frac{j}{(\omega C_P)} \quad (1a)$$

$$-\varphi = \arctan\left[\frac{1}{\omega(R_S + R_F)C_P}\right] \quad (1b)$$

for the upper circuit in Fig. 1b or

$$Z = R_S - \frac{j}{\omega(C_P + C_D)} \quad (2a)$$

$$-\varphi = \arctan\left[\frac{1}{\omega R_S(C_P + C_D)}\right] \quad (2b)$$

for the lower circuit in Fig. 1b, where j is the imaginary unit (i.e., $j^2 = -1$) and ω is the angular frequency, defined as $\omega = 2\pi f$, where f is the frequency. Under these conditions,

$$R_P \gg \frac{1}{(\omega C_P)} \text{ and } R_P \gg R_S + R_F \quad (3)$$

In the previous papers [9-15], only Eq. (1) was used with a footnote stating that C_P practically includes C_D (see Table 1 in Ref. 12, Tables 1 and 2 in Ref. 13, etc.). Both Eqs. (1) and (2) show that the effect of R_P on $-\varphi$ for intermediate frequencies is negligible. These aspects are completely overlooked, confused, and misunderstood in the comments on the phase-shift method [18-20]. Correspondingly, all of the simulations on the phase-shift method using Eq. (1), which appears in the comments (C_P does not include C_D), are basically invalid and incorrect. All of the analyses of the effect of R_P on $-\varphi$ for intermediate frequencies are meaningless (see Supporting Information in Ref. 18).

The following limitations and conditions of the equivalent circuit elements for f_o are summarized on the basis of the experimental data in the previous papers [9-20]. Neither R_S nor C_D is constant. At $\theta \approx 0$, $R_S > R_F$ and $C_D > C_P$, or vice versa, and so forth. For a wide range of θ (i.e., $0.2 < \theta < 0.8$), $R_F >> R_S$ or $R_F > R_S$ and $C_P >> C_D$ or $C_P > C_D$, and so forth. At $\theta \approx 1$, $R_S > R_F$ or $R_S < R_F$ and $C_P >> C_D$. The measured φ for f_o depends on E and θ. In contrast to numerical simulations, the limitations and conditions for Eq. (1) or (2) are not considered for the phase-shift method because all of the measured values of $-\varphi$ for intermediate frequencies include (R_S, R_F) and (C_P, C_D). Correspondingly, the measured $-\varphi$ for f_o is valid and correct regardless of the applicability of Eq. (1) or (2). Both the measured values of $-\varphi$ at f_o and the calculated values of $-\varphi$ at f_o using Eq. (1) or (2) are exactly the same (see Supporting Information in Ref. 18). The unique feature and combination of (R_S, R_F) and (C_P, C_D) vs. E for f_o are equivalent to those of R_ϕ and C_ϕ vs. E for f_o, i.e., $-\varphi$ and θ vs. E for f_o, due to the reciprocal property of R_F and C_P, which include R_ϕ and C_ϕ. It suggests that only the polar form of the equivalent circuit impedance, i.e., $-\varphi$ described in Eq. (1b) or (2b), is useful and effective for studying the linear relationship between the $-\varphi$ ($90° \geq -\varphi \geq 0°$) vs. E behavior at f_o and the θ ($0 \leq \theta \leq 1$) vs. E behavior. The linear relationship between the Gaussian profiles of $\Delta(-\varphi)/\Delta E$ and $\Delta\theta/E$ for f_o implies that only one Frumkin or Langmuir adsorption isotherm is determined on the basis of the relevant experimental results (see Figs. 2, 7 to 9). The shape and location of the (θ vs. E) profile for f_o correspond to g and K for the Frumkin or Langmuir adsorption isotherm (see Figs. 7b, 8, and 10c). These aspects are the essential nature of the phase-shift method for determining the Frumkin and Langmuir adsorption isotherms.

3. Basic Procedure and Description of the Phase-Shift Method

3-1. The phase-shift curves ($-\varphi$ vs. log f) for different potentials

Figure 2 compares the phase-shift curves ($-\varphi$ vs. log f) for differ-

Table 1. Measured values of the phase shift ($-\varphi$) for f_o = 1.259 Hz, the fractional surface coverage (θ) of OPD H and OPD D, and the normalized rates of change of $-\varphi$ and θ vs. E [$\Delta(-\varphi)/\Delta E$, $\Delta\theta/\Delta E$] at the Pt-Ir alloy/0.1 M LiOH (H_2O + D_2O) solution interface

E/V vs. SHE[a]	$-\varphi$/deg	θ[b]	$\Delta(-\varphi)/\Delta E$[c]	$\Delta\theta/\Delta E$[d]
−0.659	84.7	~ 0	~ 0	~ 0
−0.684	84.0	0.00830	0.08304	0.08304
−0.709	79.4	0.06287	0.54567	0.54567
−0.734	60.8	0.28351	2.20641	2.20641
−0.759	26.6	0.68921	4.05694	4.05694
−0.784	7.7	0.91340	2.24199	2.24199
−0.809	2.6	0.97390	0.60498	0.60498
−0.834	1.3	0.98932	0.15421	0.15421
−0.859	0.7	0.99644	0.07117	0.07117
−0.884	0.6	0.99763	0.01186	0.01186
−0.909	0.4	~ 1	0.02372	0.02372

[a]SHE (standard hydrogen electrode). [b]$0 \leq \theta \leq 1$. [c]{[(neighbor phase shift difference)/(total phase shift difference)]/[(neighbor potential difference)/(total potential difference)]}. [d]{[(neighbor fractional surface coverage difference)/(total fractional surface coverage difference)]/[(neighbor potential difference)/(total potential difference)]}

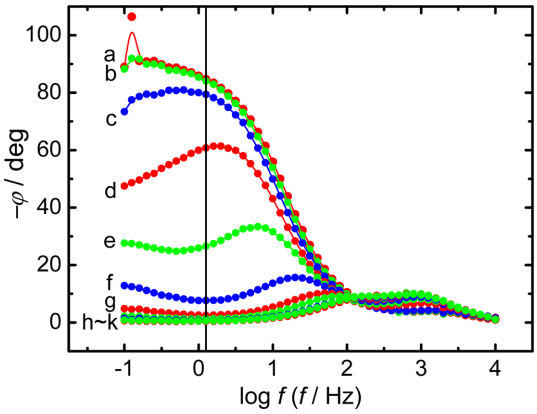

Fig. 2. Comparison of the phase-shift curves ($-\varphi$ vs. log f) for different potentials (E) at the Pt-Ir alloy/0.1 M LiOH (H_2O + D_2O) solution interface [20]. Measured values: ●. Vertical solid line: 1.259 Hz; single sine wave; scan frequency range, (10^4 to 0.1) Hz; ac amplitude, 5 mV. Dc potentials: (a) –0.659 V, (b) –0.684 V, (c) –0.709 V, (d) –0.734 V, (e) –0.759 V, (f) –0.784 V, (g) –0.809 V, (h) –0.834 V, (i) –0.859 V, (j) –0.884 V, and (k) –0.909 V (all vs. SHE).

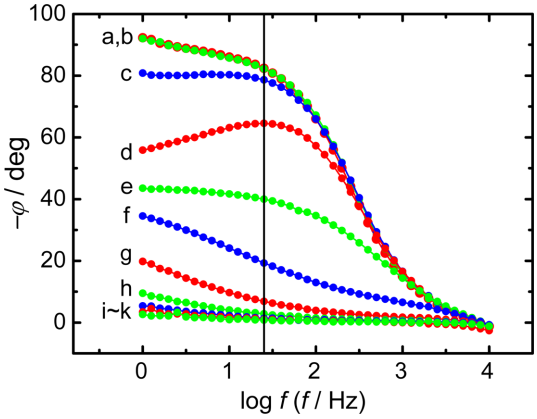

Fig. 3. Comparison of the phase-shift curves ($-\varphi$ vs. log f) for different potentials (E) at the Pt-Ir alloy/0.5 M H_2SO_4 aqueous solution interface [19]. Measured values: ●. Vertical solid line: 25.12 Hz; single sine wave; scan frequency range, (10^4 to 1) Hz; ac amplitude, 5 mV. Dc potentials: (a) 0.061 V, (b) 0.041 V, (c) 0.021 V, (d) 0.001 V, (e) –0.019 V, (f) –0.039 V, (g) –0.059 V, (h) –0.079 V, (i) –0.099 V, (j) –0.119 V, and (k) –0.139 V (all vs. SHE).

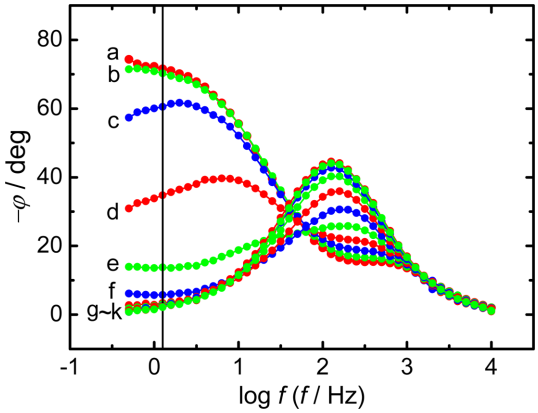

Fig. 4. Comparison of the phase-shift curves ($-\varphi$ vs. log f) for different potentials (E) at the Ir/0.1 M KOH aqueous solution interface [16]. Measured value: ●. Vertical solid line: 1.259 Hz; single sine wave; scan frequency range, (10^4 to 0.5) Hz; ac amplitude, 5 mV. Dc potential: (a) –0.659 V, (b) –0.684 V, (c) –0.709 V, (d) –0.734 V, (e) –0.759 V, (f) –0.784 V, (g) –0.809 V, (h) –0.834 V, (i) –0.859 V, (j) –0.884 V, and (k) –0.909 V (all vs. SHE).

ent E at the Pt-Ir alloy/0.1 M LiOH (H_2O + D_2O) solution interface [20]. The intermediate frequency of 1.259 Hz, shown as a vertical solid line on the ($-\varphi$ vs. log f) plot in Fig. 2, can be set as f_o for ($-\varphi$ vs. E) and (θ vs. E) profiles. All E in Table 1 and Figs. 2~19 are given on the standard hydrogen electrode (SHE) scale. The following qualitative interpretation is valid and effective for studying the linear relationship between $\Delta(-\varphi)/\Delta E$ and $\Delta\theta/\Delta E$ for f_o at noble metal and alloy/solution interfaces [8-21].

At the maximum $-\varphi$ shown in curve a of Fig. 2, it appears that the adsorption of OPD H and OPD D and superposition of various effects are minimized; i.e., $\theta \approx 0$ and E is low. At the maximum $-\varphi$, when $\theta \approx 0$ and E is low, both $\Delta(-\varphi)/\Delta E$ and $\Delta\theta/\Delta E$ for f_o are minimized because (R_ϕ and C_ϕ vs. E) approach minimum values or 0. At the minimum $-\varphi$ shown in curve k of Fig. 2, it appears that the adsorption of OPD H and OPD D and superposition of various effects are maximized or almost saturated; i.e., $\theta \approx 1$ and E is high. At the minimum $-\varphi$, when $\theta \approx 1$ and E is high, both $\Delta(-\varphi)/\Delta E$ and $\Delta\theta/\Delta E$ for f_o are also minimized because (R_ϕ and C_ϕ vs. E) approach minimum values or 0. At the medium $-\varphi$ between curves d and e in Fig. 2, it appears that both $\Delta(-\varphi)/\Delta E$ and $\Delta\theta/\Delta E$ for f_o are maximized because (R_ϕ and C_ϕ vs. E) approach maximum values at $\theta \approx 0.5$ and intermediate E. At other values of φ in Fig. 2, both $\Delta(-\varphi)/\Delta E$ and $\Delta\theta/\Delta E$ for f_o decrease symmetrically with E because (R_ϕ and C_ϕ vs. E) decrease symmetrically with E at other values of θ (see Table 1 and Fig. 9b). Therefore, one can obtain the linear relationship between the Gaussian profiles of $\Delta(-\varphi)/\Delta E$ and $\Delta\theta/\Delta E$ for f_o on the basis of the relevant phase-shift curves ($-\varphi$ vs. log f) for different E. Similarly, Figs. 3, 4, 5, and 6 show the phase-shift curves ($-\varphi$ vs. log f) for different E at the Pt-Ir [19], Ir [16], Pd [12], and Au [10] interfaces, respectively.

Note that $-\varphi$ depends on both E and f but θ depends on only E. This is the reason why a single equation for ($-\varphi$ vs. θ) as functions of E and f is necessary. However, the phase-shift method has been experimentally proposed and verified on the basis of the phase-shift curves ($-\varphi$ vs. log f) at different E (see Figs. 2 to 6). The electrochemical impedance data, i.e., ($-\varphi$ vs. log f) and ($-\varphi$ vs. E), were measured and interpreted by using the frequency response analyzer and EIS. In practice, the cyclic, differential pulse, and linear sweep voltammetries are not necessary for the phase-shift method itself [10-12].

3-2. The phase-shift ($-\varphi$ vs. E) and fractional surface coverage (θ vs. E) profiles

The procedure and description of the phase-shift method for determining the Frumkin adsorption isotherm of OPD H and OPD D at the Pt-Ir alloy/0.1 M LiOH (H_2O + D_2O) solution interface are summarized in Table 1 [20].

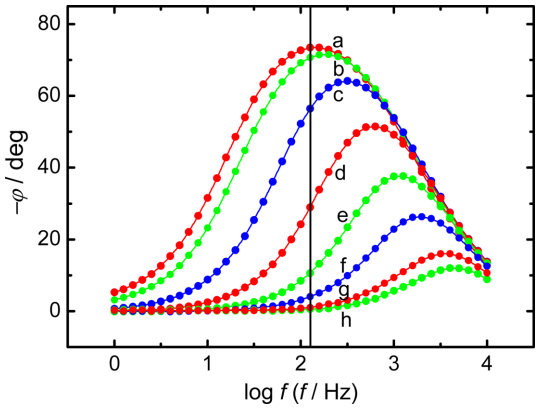

Fig. 5. Comparison of the phase-shift curves ($-\varphi$ vs. log f) for different potentials (E) at the Pd/0.5 M H_2SO_4 aqueous solution interface [adapted from Ref. 12]. Measured value: ●. Vertical solid line: 125.9 Hz; single sine wave; scan frequency range, (10^4 to 1) Hz; ac amplitude, 5 mV. Dc potential: (a) 0.066 V, (b) 0.016 V, (c) −0.034 V, (d) −0.084 V, (e) −0.134 V, (f) −0.184 V, (g) −0.259 V, and (h) −0.309 V (all vs. SHE).

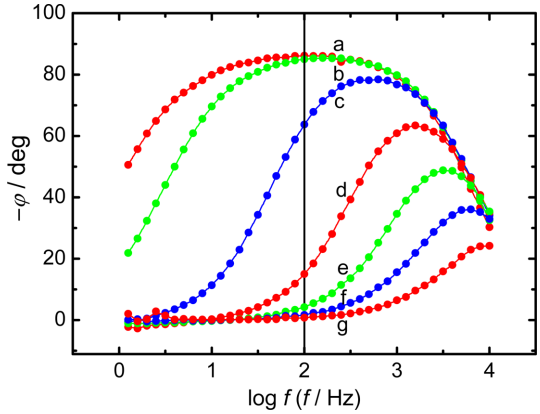

Fig. 6. Comparison of the phase-shift curves ($-\varphi$ vs. log f) for different potentials (E) at the Au/0.5 M H_2SO_4 aqueous solution interface [adapted from Ref. 10]. Measured value: ●. Vertical solid line: 100 Hz; single sine wave; scan frequency range, (10^4 to 1) Hz; ac amplitude, 5 mV. Dc potential: (a) −0.009 V, (b) −0.059 V, (c) −0.109 V, (d) −0.159 V, (e) −0.209 V, (f) −0.259 V, and (g) −0.309 V (all vs. SHE).

The values of $-\varphi$ and θ as a function of E at f_o = 1.259 Hz shown in Fig. 7 [20] are illustrated on the basis of the experimental results summarized in Table 1. The values of $-\varphi$ and θ as a function of E at f = 0.1 Hz, 10 Hz, and 100 Hz shown in Fig. 7 are also illustrated through the same procedure summarized in Table 1. However, note that the differences between the ($-\varphi$ vs. E) profile at f_o = 1.259 Hz and the ($-\varphi$ vs. E) profiles at f = 0.1 Hz, 10 Hz, and 100 Hz shown in Fig. 7a do not represent the measurement error but only the frequency response. In practice, the (θ vs. E) profiles at f = 0.1 Hz, 10 Hz, and 100 Hz shown in Fig. 7b should be exactly the same as the (θ vs. E) profile at f_o = 1.259 Hz. Because, as stated above, θ depends on only E and this unique feature most clearly appears at f_o. In Table 1, the fitted range of θ does not influence the determination of the Frumkin adsorption isotherm of OPD H and OPD D. Because, as shown in Fig. 8 [20], only one Frumkin adsorption isotherm (θ vs. E) is determined regardless of the fitted range of θ over the same potential range.

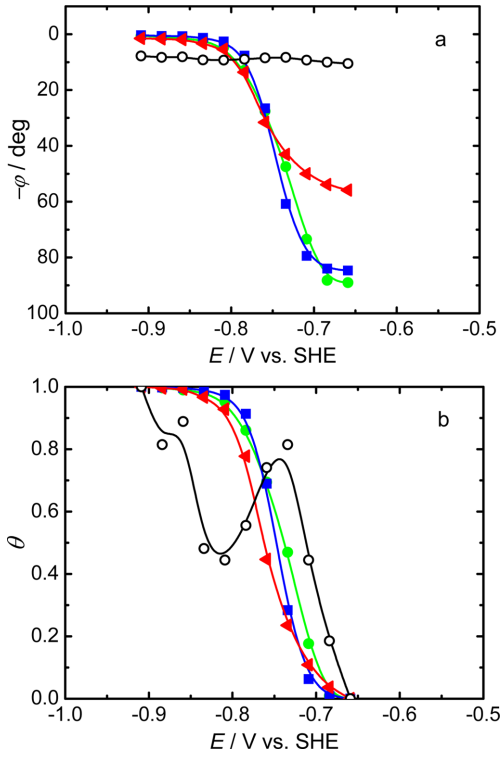

Fig. 7. Comparison of (a) the phase-shift profiles ($-\varphi$ vs. E) and (b) the fractional surface coverage profiles (θ vs. E) for four different frequencies at the Pt-Ir alloy/0.1 M LiOH (H_2O + D_2O) solution interface [20]. Experimental data: ●, 0.1 Hz; ■, 1.259 Hz; ◀, 10 Hz; ○, 100 Hz. The optimum intermediate frequency (f_o) is 1.259 Hz.

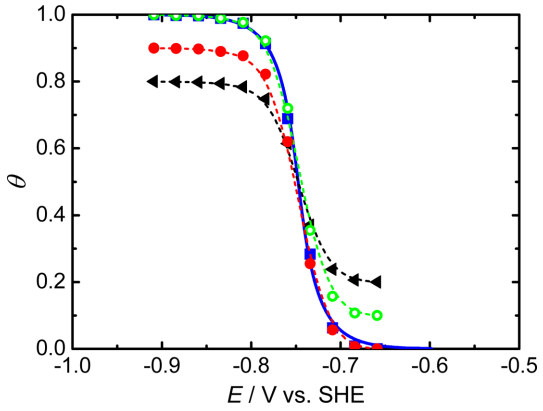

Fig. 8. Evaluation of the fitted range of θ at the Pt-Ir alloy/0.1 M LiOH (H_2O + D_2O) solution interface [adapted from Ref. 20]. Experimental data: ■ ($0 \le \theta \le 1$). Fitted data: ●, $0 \le \theta$ 0.9; ○, $0.1 \le \theta \le 1$; ◀, $0.2 \le \theta \le 0.8$. The solid curve ($0 \le \theta \le 1$) shows the Frumkin adsorption isotherm calculated using Eq. (4) for g = −2.2 with $K_o = 5.3 \times 10^{-5}$ mol^{-1}, i.e., $K = 5.3 \times 10^{-5}$ exp(2.2θ) mol^{-1}.

The normalized rates of change of $-\varphi$ and θ with respect to E, i.e., $\Delta(-\varphi)/\Delta E$ and $\Delta\theta/\Delta E$, for four different frequencies at the Pt-Ir alloy/0.1 M LiOH (H_2O + D_2O) solution interface are shown in Fig. 9 [20]. The Gaussian profile shown in Fig. 9b is illustrated on the basis of $\Delta(-\varphi)/\Delta E$ and $\Delta\theta/\Delta E$ data for f_o = 1.259 Hz summarized in Table 1. The Gaussian profiles of $\Delta(-\varphi)/\Delta E$ and $\Delta\theta/\Delta E$ at f = 0.1 Hz, 10 Hz,

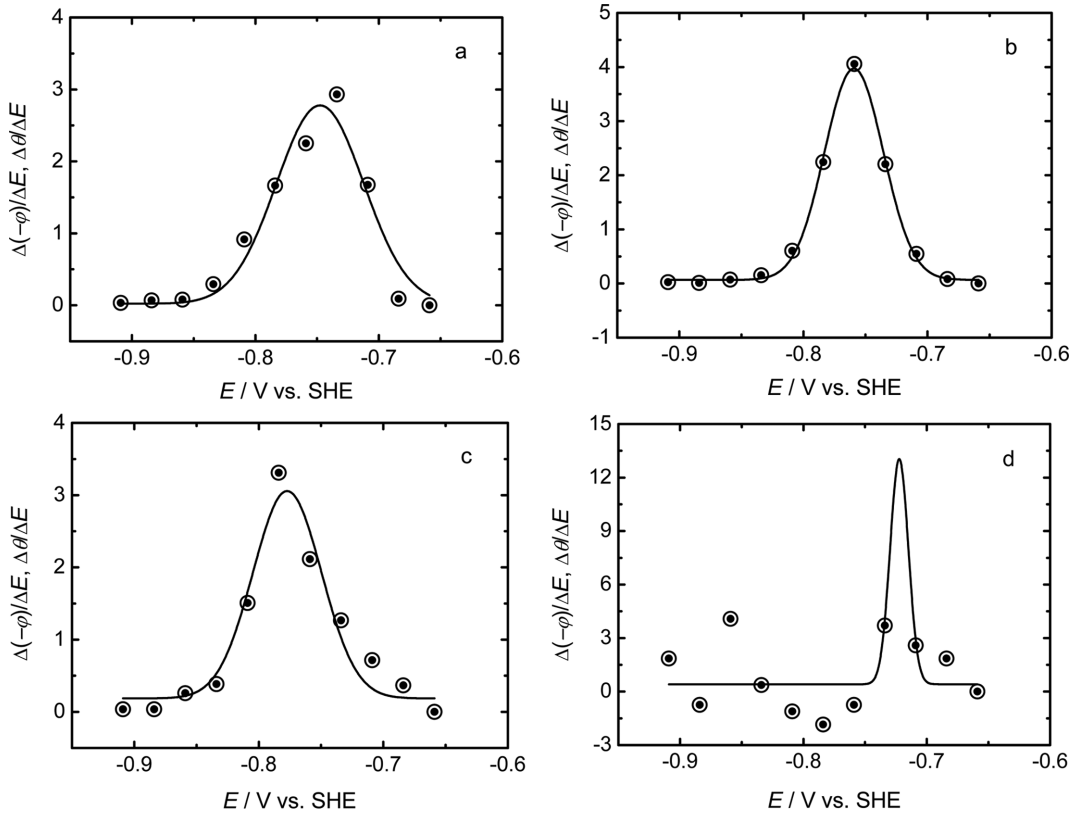

Fig. 9. Comparison of the normalized rates of change of $-\varphi$ and θ with respect to E, i.e., $\Delta(-\varphi)/\Delta E$ and $\Delta\theta/\Delta E$, for four different frequencies at the Pt-Ir alloy/0.1 M LiOH ($H_2O + D_2O$) solution interface [20]. Solid curves show the fitted Gaussian profiles. Experimental data: ○, $\Delta(-\varphi)/\Delta E$; ●, $\Delta\theta/\Delta E$. (a) 0.1 Hz, (b) 1.259 Hz, (c) 10 Hz, and (d) 100 Hz. The optimum intermediate frequency (f_o) is 1.259 Hz.

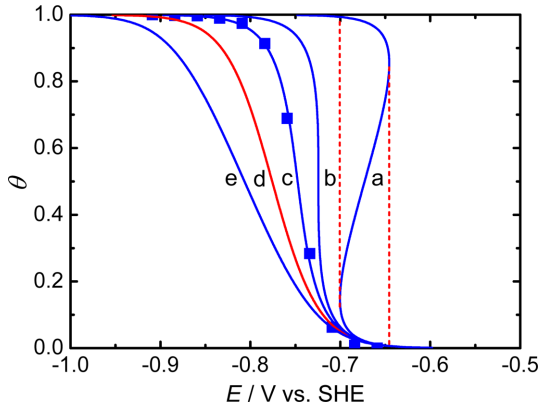

Fig. 10. Comparison of the five fitted data for the Frumkin adsorption isotherms at the Pt-Ir alloy/0.1 M LiOH ($H_2O + D_2O$) solution interface [adapted from Ref. 20]. Experimental data: ■. Solid curves show the Frumkin adsorption isotherms (θ vs. E) calculated using Eq. (4) for (a) g = –8, (b) g = –4, (c) g = –2.2, (d) g = 0, i.e., the Langmuir adsorption isotherm, and (e) g = 2.4 with $K_o = 5.3 \times 10^{-5}$ mol^{-1}. Dashed lines show the hysteresis loop of two-dimensional phase formation.

and 100 Hz are shown in Figs. 9a, c, and d, respectively. Finally, one can conclude that the (θ vs. E) and $\Delta\theta/\Delta E$ profiles at f_o = 1.259 Hz shown in Figs. 7b and 9b, respectively, are applicable to the determination of the Frumkin adsorption isotherm of OPD H and OPD D at the interface (see Fig. 10).

4. Electrochemical Frumkin, Langmuir, and Temkin Adsorption Isotherms

4-1. The Frumkin and Langmuir adsorption isotherms

The derivation and interpretation of the practical forms of the electrochemical Frumkin, Langmuir, and Temkin adsorption isotherms are described elsewhere [1,2,26]. The Frumkin adsorption isotherm assumes that the surface is inhomogeneous or that the lateral interaction effect is not negligible. It is well known that the Langmuir adsorption isotherm is a special case of the Frumkin adsorption isotherm. The Langmuir adsorption isotherm can be derived from the Frumkin adsorption isotherm by setting the interaction parameter (g) to be zero, i.e., g = 0. The Frumkin adsorption isotherm (θ vs. E) can be expressed as follows [26]

$$\left[\frac{\theta}{1-\theta}\right]\exp(g\theta) = K_o C^+ \exp(-EF/RT) \tag{4}$$

$$g = \frac{r}{RT} \tag{5}$$

$$K = K_o \exp(-g\theta) \tag{6}$$

where θ ($0 \le \theta \le 1$) is the fractional surface coverage, g is the interaction parameter for the Frumkin adsorption isotherm, K_o is the equilibrium constant at g = 0, C^+ is the concentration of ions (H^+, D^+, $H^+ + D^+$, etc.) in the bulk solution, E is the applied

potential, F is Faraday's constant, R is the gas constant, T is the absolute temperature, r is the rate of change of the standard Gibbs energy (ΔG_θ°) of adsorption with θ ($0 \le \theta \le 1$), and K is the equilibrium constant. Note that when g = 0 in Eqs. (4) to (6), the Langmuir adsorption isotherm is obtained. For the Langmuir adsorption isotherm, when g = 0, the inhomogeneous and lateral interaction effects are assumed to be negligible.

Figure 10 shows the determination of the Frumkin adsorption isotherm of OPD H and OPD D using Eq. (4) at the Pt-Ir alloy/0.1 M LiOH (H_2O + D_2O) solution interface [20]. Curves a, b, c, d, and e show the five numerically calculated Frumkin adsorption isotherms corresponding to g = –8, –4, –2.2, 0, and 2.4, respectively, for K_o = 5.3×10^{-5} mol^{-1}. The curve c shows that the Frumkin adsorption isotherm, $K = 5.3 \times 10^{-5} \exp(2.2\theta)$ mol^{-1}, is applicable to the adsorption of OPD H and OPD D, and Eq. (5) gives r = –5.5 kJ mol^{-1}. The Frumkin adsorption isotherm implies that the lateral interaction between OPD H and OPD D species is not negligible. In other words, the Langmuir adsorption isotherm for g = 0, i.e., $K = 5.3 \times 10^{-5}$ mol^{-1}, is not applicable to the adsorption of OPD H and OPD D at the interface (see Fig. 10d).

Figures 11, 12, and 13 also show the determination of the Frumkin adsorption isotherms of OPD H using Eq. (4) at the Pt [14], Ir [14], and Pd [12] interfaces, respectively. Similarly, Fig. 14 shows the determination of the Langmuir adsorption isotherm of OPD H using Eq. (4) for g = 0 at the Au interface [10]. As stated above, the Langmuir adsorption isotherm implies that the lateral interaction between OPD H species is negligible.

4-2. The Temkin adsorption isotherm

At intermediate values of θ, i.e., $0.2 < \theta < 0.8$, the pre-exponential term, $[\theta(1 - \theta)]$, varies little with θ in comparison with the variation of the exponential term, $\exp(g\theta)$. Under these approximate conditions, the Temkin adsorption isotherm can be simply derived from the Frumkin adsorption isotherm. The Temkin adsorption isotherm (θ vs. E)

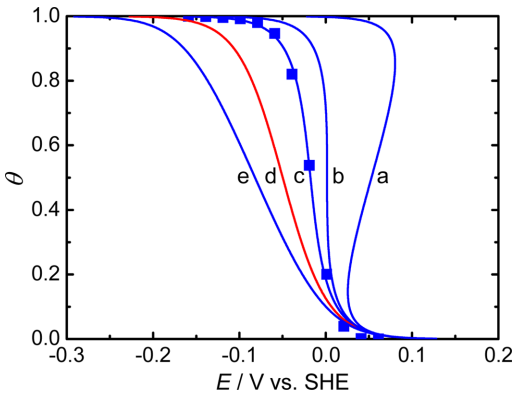

Fig. 11. Comparison of the five fitted Frumkin adsorption isotherms at the Pt/0.5 M H_2SO_4 aqueous solution interface [adapted from Ref. 14]. Experimental data: ■. Solid curves show the Frumkin adsorption isotherms (θ vs. E) calculated using Eq. (4) for (a) g = –8, (b) g = –4, (c) g = –2.5, (d) g = 0, i.e., the Langmuir adsorption isotherm, and (e) g = 2.5 with K_o = 3.5×10^{-5} mol^{-1}.

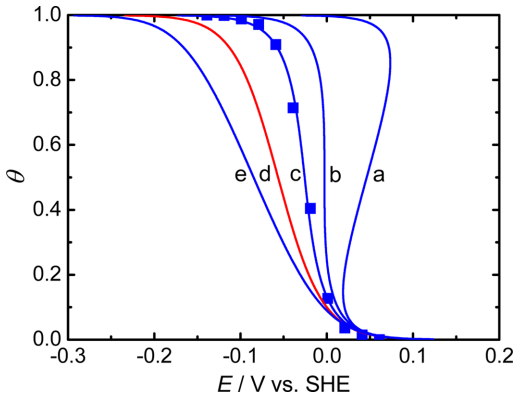

Fig. 12. Comparison of the five fitted Frumkin adsorption isotherms at the Ir/0.5 M H_2SO_4 aqueous solution interface [adapted from Ref. 14]. Experimental data: ■. Solid curves show the Frumkin adsorption isotherms (θ vs. E) calculated using Eq. (4) for (a) g = –8, (b) g = –4, (c) g = –2.4, (d) g = 0, i.e., the Langmuir adsorption isotherm, and (e) g = 2.4 with K_o = 2.7×10^{-5} mol^{-1}.

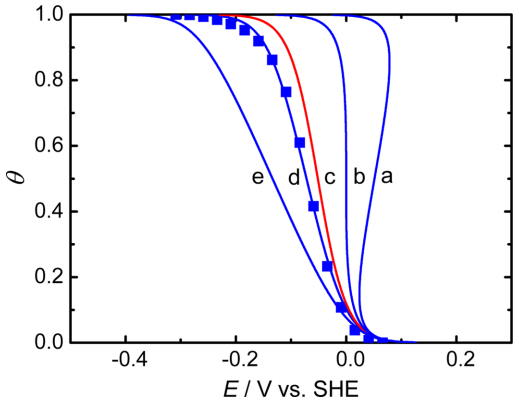

Fig. 13. Comparison of the five fitted Frumkin adsorption isotherms at the Pd/0.5 M H_2SO_4 aqueous solution interface [adapted from Ref. 12]. Experimental data: ■. Solid curves show the Frumkin adsorption isotherms (θ vs. E) calculated using Eq. (4) for (a) g = –8, (b) g = –4, (c) g = 0, i.e., the Langmuir adsorption isotherm, (d) g = 1.6, and (e) g = 6.4 with K_o = 3.3×10^{-5} mol^{-1}.

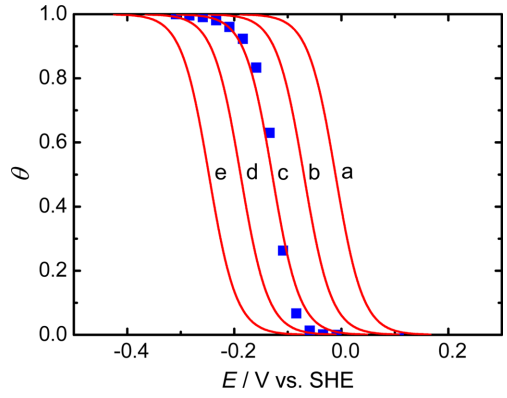

Fig. 14. Comparison of the five fitted Langmuir adsorption isotherms at the Au/0.5 M H_2SO_4 aqueous solution interface [adapted from Ref. 10]. Experimental data: ■. Solid curves show the Langmuir adsorption isotherms (θ vs. E) calculated using Eq. (4) for g = 0. (a) $K = 2.3 \times 10^{-4}$ mol^{-1}, (b) $K = 2.3 \times 10^{-5}$ mol^{-1}, (c) $K = 2.3 \times 10^{-6}$ mol^{-1}, (d) $K = 2.3 \times 10^{-7}$ mol^{-1}, and (e) $K = 2.3 \times 10^{-8}$ mol^{-1}.

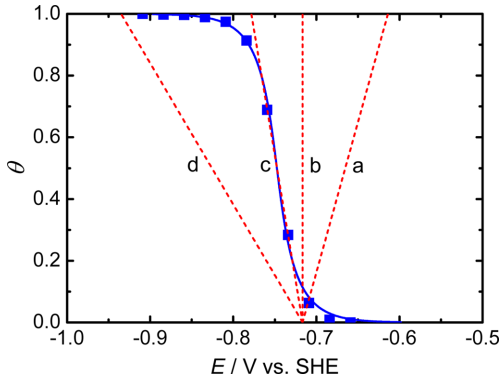

Fig. 15. Comparison of the Frumkin and four fitted Temkin adsorption isotherms at the Pt-Ir alloy/0.1 M LiOH (H_2O + D_2O) solution interface [adapted from Ref. 20]. Experimental data: ■ . The solid curve shows the Frumkin adsorption isotherm, i.e., $K = 5.3 \times 10^{-5} \exp(2.2\theta)$ mol^{-1}. Dashed lines show the Temkin adsorption isotherms (θ vs. E) calculated using Eq. (7) and the correlation constants for (a) g = –4, (b) g = 0, (c) g = 2.4, and (d) g = 8.5 with $K_0 = 5.3 \times 10^{-4}$ mol^{-1}. Note that the Temkin adsorption isotherm, i.e., $K = 5.3 \times 10^{-4} \exp(-2.4\theta)$ mol^{-1}, is valid and effective only at $0.2 < \theta < 0.8$.

can be expressed as follows [26].

$$\exp(g\theta) = K_0 C^+ \exp(-EF/RT) \quad (7)$$

The physical meaning of g in the Temkin adsorption isotherm is significantly different from that in the Frumkin adsorption isotherm. Note that g in Eq. (7) is practically determined by the slope of experimental data for $0.2 < \theta < 0.8$ (see Figs. 15 to 19). The evaluation of the applicability of the Frumkin and Temkin adsorption isotherms over the same potential range is described elsewhere [16,20].

Figure 15 shows the determination of the Temkin adsorption isotherm corresponding to the Frumkin adsorption isotherm shown in curve c of Fig. 10. The dashed line labeled c in Fig. 15 shows that the numerically calculated Temkin adsorption isotherm of OPD H and OPD D using Eq. (7) is $K = 5.3 \times 10^{-4} \exp(-2.4\theta)$ mol^{-1}, and Eq. (5) gives $r = 6.0$ kJ mol^{-1}.

Figures 16, 17, and 18 also show the determination of the Temkin adsorption isotherms corresponding to the Frumkin adsorption isotherms shown in Figs. 11c, 12c, and 13d, respectively. Similarly, Fig. 19 shows the determination of the Temkin adsorption isotherm corresponding to the Langmuir adsorption isotherm shown in Fig. 14c. The g and K for the Frumkin and Temkin adsorption isotherms of OPD H and OPD D at the noble metal and alloy/H_2O and D_2O solution interfaces are summarized in Table 2.

4-3. The correlation constants between the Temkin and Frumkin or Langmuir adsorption isotherms

For $0.2 < \theta < 0.8$, all the Langmuir adsorption isotherms are parallel to each other (see Fig. 14). Correspondingly, all the slopes of the Langmuir adsorption isotherms, i.e., all g for the Temkin adsorption isotherms, are the same regardless of the values of K. As summarized in Table 2, we have experimentally found that the values of g for the Temkin adsorption isotherms are approximately 4.6 greater than those for the Langmuir adsorption isotherms (see Fig. 19). Similarly, the values of g for the Temkin adsorption isotherms are approximately 4.6 greater than those for the Frumkin adsorption isotherms (see Figs. 15 to 18). Because the Frumkin adsorption isotherm is determined on the basis of the Langmuir adsorption isotherm (see Figs. 10 to 13). In addition, we have experimentally found that K_0 for the Temkin adsorption isotherm is approximately 10 times greater than K_0 for the correlated Frumkin or Langmuir adsorption isotherm (see Figs. 15 to 19 and Table 2). The values of g and K_0 for the Temkin adsorption isotherm are approximately 4.6 and 10 times greater than those for the correlated Frumkin or Langmuir adsorption isotherm, respectively. These factors (ca. 4.6 and 10) can be taken as correlation constants between the Temkin and Frumkin or Langmuir adsorption isotherms.

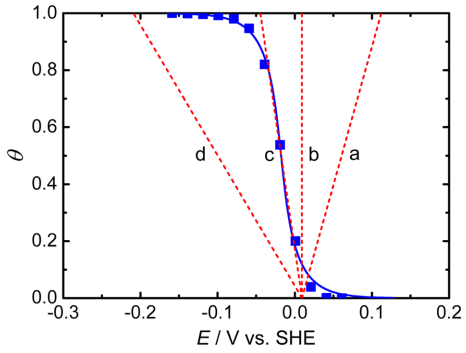

Fig. 16. Comparison of the Frumkin and four fitted Temkin adsorption isotherms at the Pt/0.5 M H_2SO_4 aqueous solution interface [adapted from Ref. 14]. Experimental data: ■. The solid curve shows the Frumkin adsorption isotherm, i.e., $K = 3.5 \times 10^{-5} \exp(2.5\theta)$ mol^{-1}. Dashed lines show the Temkin adsorption isotherms (θ vs. E) calculated using Eq. (7) and the correlation constants for (a) g = –4, (b) g = 0, (c) g = 2.1, and (d) g = 8.5 with $K_0 = 3.5 \times 10^{-4}$ mol^{-1}. Note that the Temkin adsorption isotherm, i.e., $K = 3.5 \times 10^{-4} \exp(-2.1\theta)$ mol^{-1}, is valid and effective only at $0.2 < \theta < 0.8$.

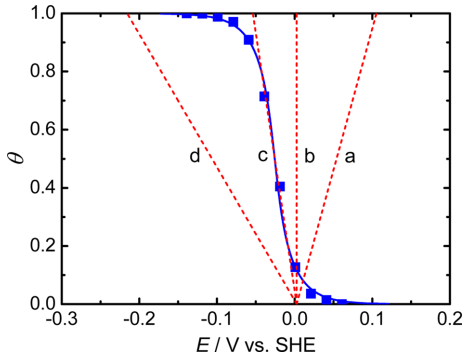

Fig. 17. Comparison of the Frumkin and four fitted Temkin adsorption isotherms at the Ir/0.5 M H_2SO_4 aqueous solution interface [adapted from Ref. 14]. Experimental data: ■. The solid curve shows the Frumkin adsorption isotherm, i.e., $K = 2.7 \times 10^{-5} \exp(2.4\theta)$ mol^{-1}. Dashed lines show the Temkin adsorption isotherms (θ vs. E) calculated using Eq. (7) and the correlation constants for (a) g = –4, (b) g = 0, (c) g = 2.2, and (d) g = 8.5 with $K_0 = 2.7 \times 10^{-4}$ mol^{-1}. Note that the Temkin adsorption isotherm, i.e., $K = 2.7 \times 10^{-4} \exp(-2.2\theta)$ mol^{-1}, is valid and effective only at $0.2 < \theta < 0.8$.

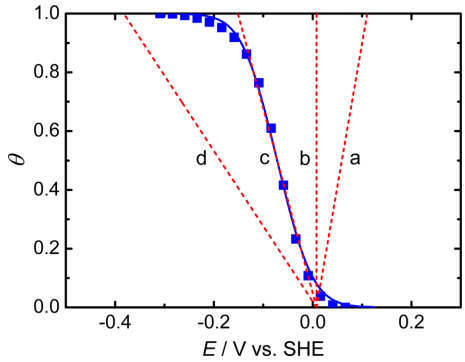

Fig. 18. Comparison of the Frumkin and four fitted Temkin adsorption isotherms at the Pd/0.5 M H_2SO_4 aqueous solution interface [adapted from Ref. 12]. Experimental data: ■. The solid curve shows the Frumkin adsorption isotherm, i.e., $K = 3.3 \times 10^{-5} \exp(-1.6\theta)$ mol^{-1}. Dashed lines show the Temkin adsorption isotherms (θ vs. E) calculated using Eq. (7) and the correlation constants for (a) g = –4, (b) g = 0, (c) g = 6.2, and (d) g = 15.2 with $K_o = 3.3 \times 10^{-4}$ mol^{-1}. Note that the Temkin adsorption isotherm, i.e., $K = 3.3 \times 10^{-4} \exp(-6.2\theta)$ mol^{-1}, is valid and effective only at $0.2 < \theta < 0.8$.

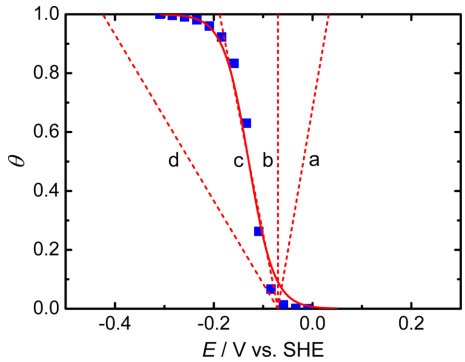

Fig. 19. Comparison of the Langmuir and four fitted Temkin adsorption isotherms at the Au/0.5 M H_2SO_4 aqueous solution interface [adapted from Ref. 10]. Experimental data: ■. The solid curve shows the Langmuir adsorption isotherm, i.e., $K = 2.3 \times 10^{-6}$ mol^{-1}. Dashed lines show the Temkin adsorption isotherms (θ vs. E) calculated using Eq. (7) and the correlation constants for (a) g = –4, (b) g = 0, (c) g = 4.6, and (d) g = 13.8 with $K_o = 2.3 \times 10^{-5}$ mol^{-1}. Note that the Temkin adsorption isotherm, i.e., $K = 2.3 \times 10^{-5} \exp(-4.6\theta)$ mol^{-1}, is valid and effective only at $0.2 < \theta < 0.8$.

Finally, one can conclude that the Temkin adsorption isotherm correlating with the Frumkin or Langmuir adsorption isotherm, and vice versa, is readily determined using the correlation constants. The two different adsorption isotherms, i.e., the Temkin and Frumkin or Langmuir adsorption isotherms, appear to fit the same data regardless of their adsorption conditions. This is a unique feature between the Temkin and Frumkin or Langmuir adsorption isotherms.

4-4. Applicability of the Langmuir and Temkin adsorption isotherms

The applicability of the Langmuir adsorption isotherm of OPD H and OPD D at the Pt-Ir alloy/0.1 M LiOH (H_2O + D_2O) solution interface is described elsewhere [20]. As shown in Figs. 10d, 11d, 12d, and 13c, the Langmuir adsorption isotherm is not applicable to the adsorption of OPD H and OPD D or OPD H at the interface. At extreme values of θ, i.e., $\theta \approx 0$ and 1, the Langmuir adsorption isotherm is often applicable to the adsorption of intermediates. However, the validity and correctness of the Langmuir adsorption isotherm are unclear and limited even at $\theta \approx 0$ and 1. As stated in the introduction, the values of g and K_o for the Frumkin adsorption isotherm are not experimentally and readily determined using other conventional methods, so the Langmuir adsorption isotherm is often used even though it has the critical limitation and applicability. To solve these problems, the phase-shift method has been originally developed [8]. In addition, the correlation constants between the Temkin and Frumkin or Langmuir adsorption isotherms have been experimentally and consistently found [12-20].

As shown in Figs. 15c, 16c, 17c, 18c, and 19c, the Temkin adsorption isotherm is valid and effective only at $0.2 < \theta < 0.8$. For $0.2 < \theta < 0.8$, note that the short potential range (ca. 28~37 mV) is difficult to observe in the Temkin adsorption isotherm correlating with the Frumkin or Langmuir adsorption isotherm. At other values of θ, i.e., $0 \le \theta < 0.2$ and $0.8 < \theta \le 1$, only the Frumkin adsorption isotherm is valid and effective. Finally, one can conclude that the Frumkin adsorption isotherm is more useful, effective, and reliable than the Langmuir and Temkin adsorption isotherms.

5. Standard Gibbs Energy of Adsorption

Under the Frumkin adsorption conditions, the relationship between the equilibrium constant (K) and the standard Gibbs energy of adsorption (ΔG°) is [26].

$$2.3RT \log K = -\Delta G_\theta^\circ \quad (8)$$

For the Pt-Ir alloy/0.1 M LiOH (H_2O + D_2O) solution interface, use of Eqs. (6) and (8) shows that ΔG_θ° of OPD H and OPD D is in the range ($24.4 \ge \Delta G_\theta^\circ \ge 18.9$) kJ mol^{-1} for $K = 5.3 \times 10^{-5} \exp(2.2\theta)$ mol^{-1} and $0 \le \theta \le 1$. This result implies an increase in the absolute value of ΔG_θ°, i.e., $|\Delta G_\theta^\circ|$, of OPD H and OPD D with θ ($0 \le \theta \le 1$). Note that ΔG_θ° is a negative number, i.e., $\Delta G_\theta^\circ < 0$ [27]. Table 3 shows ΔG_θ° of OPD H and OPD D at the noble metal and alloy/H_2O and D_2O solution interfaces.

6. Interaction Parameters for the Frumkin and Temkin Adsorption Isotherms

6-1. The negative value of the interaction parameter for the Frumkin adsorption isotherm

For the Pt, Ir, and Pt-Ir alloy interfaces [15,16,18-20], the negative values of g shown in Table 2 imply the lateral attractive ($g < 0$) interaction between OPD H and OPD D species, which leads to an increase in $|\Delta G_\theta^\circ|$ of OPD H and OPD D with θ ($0 \le \theta \le 1$) (see Table 3). This is a unique feature of OPD H and OPD D species at the interfaces.

Table 2. Comparison of the interaction parameters (g) and equilibrium constants (K) for the Frumkin and Temkin adsorption isotherms of OPD H and OPD D at the noble metal and alloy/normal (H_2O) and heavy water (D_2O) solution interfaces

Interface	Adsorbate	Frumkin		Temkin		Ref.
		g	K/mol^{-1}	g	K/mol^{-1}	
Pt-Ir alloy/0.1 M LiOH	OPD H	−2.2	$8.6 \times 10^{-5} \exp(2.2\theta)$	2.4	$8.6 \times 10^{-4} \exp(-2.4\theta)$	18
Pt-Ir alloy/0.1 M LiOH (H_2O, D_2O)	OPD H, D	−2.2	$5.3 \times 10^{-5} \exp(2.2\theta)$	2.4	$5.3 \times 10^{-4} \exp(-2.4\theta)$	20
Pt-Ir alloy/0.1 M LiOH (D_2O)	OPD D	−2.3	$2.1 \times 10^{-5} \exp(2.3\theta)$	2.3	$2.1 \times 10^{-4} \exp(-2.3\theta)$	18
Pt-Ir alloy/0.5 M H_2SO_4	OPD H	−2.5	$3.3 \times 10^{-5} \exp(2.5\theta)$	2.1	$3.3 \times 10^{-4} \exp(-2.1\theta)$	19
Pt/0.1 M KOH	OPD H	−2.4	$1.2 \times 10^{-4} \exp(2.4\theta)$	2.2	$1.2 \times 10^{-3} \exp(-2.2\theta)$	16
Pt/0.5 M H_2SO_4	OPD H	−2.5[a]	$3.5 \times 10^{-5} \exp(2.5\theta)$	2.1	$3.5 \times 10^{-4} \exp(-2.1\theta)$	14
Ir/0.1 M KOH	OPD H	−2.4	$9.4 \times 10^{-5} \exp(2.4\theta)$	2.2	$9.4 \times 10^{-4} \exp(-2.2\theta)$	16
Ir/0.5 M H_2SO_4	OPD H	−2.4	$2.7 \times 10^{-5} \exp(2.4\theta)$	2.2	$2.7 \times 10^{-4} \exp(-2.2\theta)$	14
Pd/0.5 M H_2SO_4	OPD H	1.6[a]	$3.3 \times 10^{-5} \exp(-1.6\theta)$	6.2	$3.3 \times 10^{-4} \exp(-6.2\theta)$	12
Au/0.5 M H_2SO_4	OPD H	0[b]	2.3×10^{-6}	4.6	$2.3 \times 10^{-5} \exp(-4.6\theta)$	10
Re/0.1 M KOH	OPD H	0[b]	1.9×10^{-6}	4.6	$1.9 \times 10^{-5} \exp(-4.6\theta)$	11
Re/0.5 M H_2SO_4	OPD H	0[b]	4.5×10^{-7}	4.6	$4.5 \times 10^{-6} \exp(-4.6\theta)$	11

[a]Adapted for this work. [b]Langmuir adsorption isotherm. Note that the values of g and K_o for the Temkin adsorption isotherm are approximately 4.6 and 10 times greater than those for the correlated Frumkin or Langmuir adsorption isotherm, respectively. All the Temkin adsorption isotherms are valid and effective only at $0.2 < \theta < 0.8$

Table 3. Comparison of the standard Gibbs (ΔG_θ°) energies of adsorption and the rates (r) of change of ΔG_θ° with θ ($0 \le \theta \le 1$) for the Frumkin adsorption isotherms of OPD H and OPD D at the noble metal and alloy/normal (H_2O) and heavy water (D_2O) solution interfaces

Interface	Adsorbate	ΔG_θ°/kJ mol^{-1}	r/kJ mol^{-1}	Ref.
Pt-Ir alloy/0.1 M LiOH	OPD H	$23.2 \ge \Delta G_\theta^\circ \ge 17.7$	−5.5	18
Pt-Ir alloy/0.1 M LiOH (H_2O, D_2O)	OPD H, D	$24.4 \ge \Delta G_\theta^\circ \ge 18.9$	−5.5	20
Pt-Ir alloy/0.1 M LiOH (D_2O)	OPD D	$26.7 \ge \Delta G_\theta^\circ \ge 21.0$	−5.7	18
Pt-Ir alloy/0.5 M H_2SO_4	OPD H	$25.6 \ge \Delta G_\theta^\circ \ge 19.4$	−6.2	19
Pt/0.1 M KOH	OPD H	$22.4 \ge \Delta G_\theta^\circ \ge 16.5$	−6.0	16
Pt/0.5 M H_2SO_4	OPD H	$25.4 \ge \Delta G_\theta^\circ \ge 19.2$[a]	−6.2[a]	14
Ir/0.1 M KOH	OPD H	$23.0 \ge \Delta G_\theta^\circ \ge 17.1$	−6.0	16
Ir/0.5 M H_2SO_4	OPD H	$26.1 \ge \Delta G_\theta^\circ \ge 20.1$	−6.0	14
Pd/0.5 M H_2SO_4	OPD H	$25.6 \le \Delta G_\theta^\circ \le 29.5$[a]	4.0[a]	12
Au/0.5 M H_2SO_4	OPD H	32.2[b]	0[b]	10
Re/0.1 M KOH	OPD H	32.6[b]	0[b]	11
Re/0.5 M H_2SO_4	OPD H	36.2[b]	0[b]	11

[a]Adapted for this work. [b]Langmuir adsorption isotherm

The dashed lines of Fig. 10a show that the lateral attractive ($g < 0$) interaction between OPD H and OPD D species may lead to a two-dimensional phase formation. Taking into account the critical value of g, i.e., $g = -4$ (see Fig. 10b), for the electrochemical case [27], the values of g, i.e., $g > -4$ (see Fig. 10c), shown in Table 2 are reasonable. For more negative values, i.e., $g < -4$ (see Fig. 10a), the hysteresis loop of two-dimensional phase formation will be observed. Note that $g = -4$ corresponds to $r = -9.9$ kJ mol^{-1} with $\theta (0 \le \theta \le 1)$ (see Eq. (5)). The negative values of g for the Frumkin adsorption isotherms at the Pt, Ir, and Pt-Ir alloy interfaces are qualitatively and quantitatively interpreted elsewhere [15,16,18,20].

6-2. The positive value of the interaction parameter for the Frumkin adsorption isotherm

For the Pd interface [12], the positive value of g shown in Table 2 implies the lateral repulsive ($g > 0$) interaction between OPD H species, which leads to a decrease in $|\Delta G_\theta^\circ|$ of OPD H with $\theta (0 \le \theta \le 1)$ (see Table 3). The lateral repulsive ($g > 0$) interaction between OPD H species at the Pd interface is distinctly different from the lateral attractive ($g < 0$) interaction between OPD H and OPD D species at the Pt, Ir, and Pt-Ir alloy interfaces. Note that the Pd belongs to the same Pt group metal.

For the Au and Re interfaces [10,11], the lateral interaction between OPD H species is negligible, i.e., $g = 0$ or $g \approx 0$. As previously described, this implies that the Langmuir adsorption isotherm is applicable to the adsorption of OPD H at the interfaces (see Fig. 14).

6-3. The positive value of the interaction parameter for the Temkin adsorption isotherm

Table 2 also shows that all g for the Temkin adsorption isotherms of OPD H and OPD D at the same interfaces are positive values. In other words, all the lateral interactions between OPD H and OPD D species are repulsive. It is not true except the Pd interface. As previously described, the physical meaning of g in the Temkin adsorption isotherm is significantly different from that in the Frumkin adsorption isotherm regardless of their mathematical approximations. This

is the critical limitation of the Temkin adsorption isotherm of OPD H and OPD D at the Pt group metal and alloy interfaces.

7. Summary

The Frumkin, Langmuir, and Temkin adsorption isotherms (θ vs. E) cannot be experimentally and readily determined using conventional methods. At present, the phase-shift method and correlation constants seem to be the most accurate, useful, and effective techniques for determining the Frumkin, Langmuir, and Temkin adsorption isotherms of intermediates (OPD H, OPD D, OH, etc.) for the sequential reactions (HER, DER, OER, etc.) and related electrode kinetic and thermodynamic parameters (θ vs. E, K, g, $\Delta G_{\theta}^{\circ}$, r) at electrode/normal (H_2O) and heavy water (D_2O) solution interfaces.

For the Pt, Ir, and Pt-Ir alloy interfaces, the lateral attractive ($g < 0$) interaction between OPD H and OPD D species is determined. In contrast to the Pt, Ir, and Pt-Ir alloy interfaces, the lateral repulsive ($g > 0$) interaction between OPD H species is determined at the Pd interface. For the Au and Re interfaces, the lateral interaction between OPD H species is negligible ($g = 0$ or $g \approx 0$).

For $0.2 < \theta < 0.8$, the Temkin adsorption isotherm correlating with the Frumkin or Langmuir adsorption isotherm, and vice versa, is readily determined using the correlation constants. The Temkin and Frumkin or Langmuir adsorption isotherms appear to fit the same data regardless of their adsorption conditions. This implies that the Frumkin adsorption isotherm is the most useful, suitable, and correct for studying the adsorption processes of intermediates for the sequential reactions at the interfaces.

Finally, we expect that reliable simulations with a single equation for ($-\varphi$ vs. θ) as functions of E and f or relevant experimental data for the phase-shift method and correlation constants will be obtained and interpreted using other conventional methods. We also expect that this review article should support and encourage the investigators in the fields of interfacial electrochemistry, electrode kinetics, hydrogen technology, EIS, and fuel cells.

Acknowledgments

Figures 1, 3, and 4 and the section on theoretical and experimental backgrounds of the phase-shift method were reprinted with permission from the Journal of Chemical & Engineering Data 55, 2363-2372, 5598-5607 (2010) and 56, 251-258 (2011). Copyright 2010 and 2011, the American Chemical Society (ACS). Figures 2, 7, 9 and Table 1 were appeared in the Developments in Electrochemistry (InTech, 2012). Figures 5, 11-13, 16-18 were reprinted and adapted with permission from the International Journal of Hydrogen Energy 32, 1982-1990 (2007) and 33, 4962-4965 (2008). Figures 6, 14, and 19 were reprinted and adapted with permission from the Journal of the Electrochemical Society 150, E207-217 (2003). Copyright 2003, The Electrochemical Society (ECS). The authors wish to thank the ACS, the InTech, the International Association for Hydrogen Energy (IAHE), and the ECS.

References

1. Gileadi, E., Kirowa-Eisner, E. and Penciner, J., "Interfacial electrochemistry," Addison-Wesley: Reading, MA, 1975.
2. Bockris, JO'M. and Khan, S. U. M., "Surface electrochemistry," Plenum Press: New York, 1993.
3. Conway, B. E. and Jerkiewicz, G., Eds., "Electrochemistry and materials science of cathodic hydrogen absorption and adsorption," Electrochemical Society Proceedings, Vol. 94-21; The Electrochemical Society: Pennington, NJ, 1995.
4. Jerkiewicz, G. and Marcus, P., Eds., "Electrochemical surface science and hydrogen adsorption and absorption," Electrochemical Society Proceedings, Vol. 97-16; The Electrochemical Society: Pennington, NJ, 1997.
5. Jerkiewicz, G., "Hydrogen sorption at/in electrodes," *Prog. Surf. Sci*., **57**, 137-186(1998).
6. Jerkiewicz, G., Feliu, J. M. and Popov, B. N., Eds., "Hydrogen at surface and interfaces," Electrochemical Society Proceedings, Vol. 2000-16; The Electrochemical Society: Pennington, NJ, 2000.
7. Jerkiewicz, G., "Electrochemical hydrogen adsorption and absorption. Part 1: Under-potential deposition of hydrogen," *Electrocatal*., **1**, 179-199(2010).
8. Chun, J. H., "Methods for estimating adsorption isotherms in electrochemical systems," *U.S. Patent* 6,613,218(2003).
9. Chun, J. H. and Ra, K. H., "The phase-shift method for the Frumkin adsorption isotherms at the Pd/H_2SO_4 and KOH solution interfaces," *J. Electrochem. Soc*., **145**, 3794-3798(1998).
10. Chun, J. H., Ra, K. H. and Kim, N. Y., "Langmuir adsorption isotherms of over-potentially deposited hydrogen at poly-Au and Rh/H_2SO_4 aqueous electrolyte interfaces; Qualitative analysis using the phase-shift method," *J. Electrochem. Soc.*, **150**, E207-217(2003).
11. Chun, J. H., Jeon, S. K., Ra, K. H. and Chun, J. Y., "The phase-shift method for determining Langmuir adsorption isotherms of over-potentially deposited hydrogen for the cathodic H_2 evolution reaction at poly-Re/aqueous electrolyte interfaces," *Int. J. Hydrogen Energy*, **30**, 485-499(2005).
12. Chun, J. H., Jeon, S. K. and Chun, J. Y., "The phase-shift method and correlation constants for determining adsorption isotherms of hydrogen at a palladium electrode interface," *Int. J. Hydrogen Energy*, **32**, 1982-1990(2007).
13. Chun, J. H., Kim, N. Y. and Chun, J. Y., "Determination of adsorption isotherms of hydrogen and hydroxide at Pt-Ir alloy electrode interfaces using the phase-shift method and correlation constants," *Int. J. Hydrogen Energy*, **33**, 762-774(2008).
14. Chun, J. Y. and Chun, J. H., "Correction and supplement to the determination of the optimum intermediate frequency for the phase-shift method [Chun et al., Int. J. Hydrogen Energy 30 (2005) 247-259, 1423-1436]," *Int. J. Hydrogen Energy*, **33**, 4962-4965 (2008).
15. Chun, J. Y. and Chun, J. H., "A negative value of the interaction parameter for over-potentially deposited hydrogen at Pt, Ir, and Pt-Ir alloy electrode interfaces," *Electrochem. Commun*., **11**, 744-747(2009).
16. Chun, J., Lee, J. and Chun, J. H., "Determination of adsorption

isotherms of over-potentially deposited hydrogen on platinum and iridium in KOH aqueous solution using the phase-shift method and correlation constants," *J. Chem. Eng. Data*, **55**, 2363-2372 (2010).
17. Chun, J., Kim, N. Y. and Chun, J. H., "Determination of adsorption isotherms of hydroxide and deuteroxide on Pt-Ir alloy in LiOH solutions using the phase-shift method and correlation constants," *J. Chem. Eng. Data*, **55**, 3825-3833(2010).
18. Chun, J., Kim, N. Y. and Chun, J. H., "Determination of the adsorption isotherms of hydrogen and deuterium isotopes on a Pt-Ir alloy in LiOH solutions using the phase-shift method and correlation constants," *J. Chem. Eng. Data*, **55**, 5598-5607(2010).
19. Chun, J., Kim, N. Y. and Chun, J. H., "Determination of the adsorption isotherms of over-potentially deposited hydrogen on a Pt-Ir alloy in H_2SO_4 aqueous solution using the phase-shift method and correlation constants," *J. Chem. Eng. Data*, **56**, 251-258(2011).
20. Chun, J. and Chun, J. H., In "Developments in electrochemistry," Chun, J. H. ed., InTech, Rijeka, 2012, Ch. 1, pp. 3-27 (http://www.intechopen.com/books/developments-in-electrochemistry).
21. Chun, J. and Chun, J. H., "Determination of the Frumkin and Temkin adsorption isotherms of under-potentially deposited hydrogen at Pt group metal interfaces using the standard Gibbs energy of adsorption and correlation constants," *J. Korean Electrochem. Soc*., **16**, 211-216(2013).
22. Garcia-Garcia, R., Rivera, J. G., Anta~no-Lopez, R., Casta~neda-Olivares, F. and Orozco, G., "Impedance spectra of the cathodic hydrogen evolution reaction on polycrystalline rhenium," *Int. J. Hydrogen Energy*, **41**, 4660-4669(2016).
23. Gileadi, E., Kirowa-Eisner, E. and Penciner, J., "Interfacial Electrochemistry," Addison-Wesley, Reading, MA, 1975, pp. 89-91.
24. Harrington, D. A. and Conway, B. E., "AC Impedance of Faradaic Reactions Involving Electrosorbed Intermediates-I. Kinetic theory," *Electrochim. Acta*, **32**, 1703-1712(1987).
25. Gileadi, E., "Electrode Kinetics," VCH: New York, 1993, pp. 293-296.
26. Gileadi, E., "Electrode Kinetics," VCH: New York, 1993, pp. 261-271.
27. Gileadi, E., "Electrode Kinetics," VCH: New York, 1993, pp. 303-305.